Hotspot Detection by Phase-Modulated Pump-Based Brillouin Scattering

R. Vallifuoco, E. Catalano, L. Zeni, *Member, IEEE*, and A. Minardo, *Member, IEEE*

***Abstract*— In this letter, we present an optimized configuration for high-spatial resolution hotspot detection based on stimulated Brillouin scattering. The method makes use of a Brillouin optical frequency-domain analysis (BOFDA) configuration with a phase-modulated pump. Experiments show that the proposed method provides an average SNR enhancement of ≈ 3 dB compared to a conventional BOFDA scheme making use of an intensity-modulated pump. In detail, we demonstrate hotspot detection with a temperature standard deviation of ≈ 0.15 °C, a spatial resolution of 8 mm, a measurement range of 50 m, and an acquisition rate of 0.49 Hz. We believe that the proposed method can be usefully applied for quench detection in superconducting magnet systems, where sufficient spatial and temporal resolution are required to detect incipient quenches.**

***Index Terms*— Optical fibers, Brillouin scattering, quench detection.**

I. Introduction

DISTRIBUTED optical fiber sensors are increasingly employed in a variety of applications, owing to their ability to realize distributed temperature and strain measurements with high resolution and accuracy [1]. Their advantages, such as low weight, small size, and immunity to electromagnetic interference, make them ideal candidates for the monitoring of superconducting devices, as they can be integrated into the structure and withstand the cryogenic temperatures and high magnetic fields typical of such environments. In quench detection applications, optical fiber sensors are embedded within a superconductor cable or magnet to measure strain and temperature [2]. Up to now, a few demonstrations of quench detection with distributed optical fiber sensors have been reported. In 2016, a quench detection technique has been investigated experimentally based on optical fibers interrogated by Rayleigh backscattering [3]. The authors showed that their sensor can detect the quench-induced hotspot with a spatial resolution of 5 mm, and a time delay lower than that of the voltage taps installed for comparison during the heater-induced quenches. In [4], a quench detection system was developed based on spontaneous Brillouin scattering, featuring a 5-m spatial resolution and a measurement time of ≈ 0.5 s. A much finer spatial resolution can be realized by adopting a Brillouin measurement scheme in which the acoustic wave involved in the scattering process is pre-activated [5], [6]. Recently, we have demonstrated hotspot detection at the liquid nitrogen temperature using a slope-assisted Brillouin optical frequency-domain analysis (BOFDA) configuration [7]. The system featured a spatial resolution of 16 mm, a temperature resolution of 2 °C, and an acquisition rate of 1 Hz.

In this Letter, we demonstrate that the SNR of slope assisted BOFDA measurements can be improved by ≈ 3 dB, modulating the phase, instead of the intensity, of the pump wave involved in the measurement. This modifies the shape of the Brillouin gain spectrum (BGS), making it more suitable for fast detection of small temperature variations. The reported experiments, carried out at room temperature using a laboratory setup, demonstrate that the proposed configuration represents a possible candidate for fiber-based quench detection.

II. Principle of Operation

In BOFDA systems, a modulated pump wave interacts with a continuous-wave (cw) probe wave counter-propagating along the fiber under test (FUT). When the frequency shift between the two waves falls within the so-called Brillouin gain spectrum (BGS), the probe wave acquires an intensity modulation synchronous with the pump. Measuring the magnitude and phase of the induced modulation over a range of modulation frequencies (typically using a vector network analyzer), the so-called baseband transfer function (TF) of the FUT is obtained [8], [9]. Performing an inverse Fourier transform (IFFT) of the acquired TF, the spatial distribution of the Brillouin gain along the FUT is obtained, with a spatial resolution and measurement range determined by the set of modulation frequencies [9].

In a conventional BOFDA scheme based on an intensity-modulated (IM) pump wave, the BGS has a Lorentzian shape [10]:

$$g_i(\Delta\nu) = g_{B0}\frac{\Delta\nu_B^2}{\Delta\nu_B^2 + 4\Delta\nu^2} \tag{1}$$

In Eq. (1), g_{B0} denotes the peak gain, $\Delta\nu_B$ is the Brillouin linewidth (≈30 MHz, typically) and $\Delta\nu$ is the detuning of the interaction frequency from the center of the BGS.

Conventional static temperature (or strain) measurements are performed by scanning the pump-probe frequency shift over a proper range to reconstruct the BGS at each position. The peak frequency of the BGS (the so-called Brillouin

Manuscript received 3 August 2023; revised 24 October 2023; accepted 24 November 2023. Date of publication 27 November 2023; date of current version 15 December 2023. *(Corresponding author: A. Minardo.)*

The authors are with the Department of Engineering, University of Campania Luigi Vanvitelli, 81031 Aversa, Italy (e-mail: aldo.minardo@unicampania.it).

Color versions of one or more figures in this letter are available at https://doi.org/10.1109/LPT.2023.3337003.

Digital Object Identifier 10.1109/LPT.2023.3337003

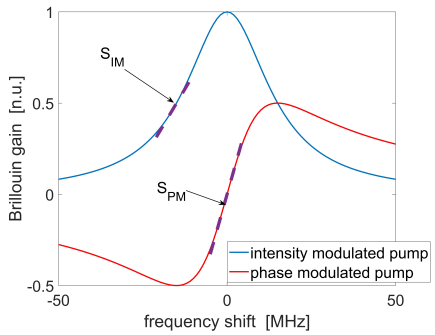

Fig. 1. Brillouin gain spectrum (BGS) for an IM (blue curve), or PM (red curve) pump.

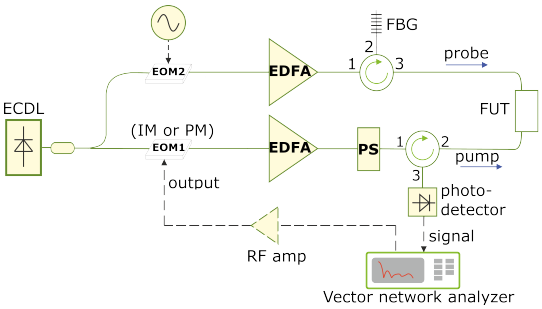

Fig. 2. Schematic of the experimental setup used for hotspot measurements.

frequency shift, BFS) shifts with temperature and strain, thus providing a mean to determine the spatial distribution of these quantities. When a high temporal resolution is required as in quench detection applications, the time-consuming sweep of the probe frequency can be avoided by resorting to a slope-assisted configuration [10], [11], [12]. In this case, the pump-probe frequency shift is kept fixed to a specific point of the BGS, while the Brillouin gain variations are recorded over consecutive acquisitions. The sensitivity is determined by the slope of the BGS at the chosen setpoint. As indicated in Fig. 1 (blue curve), the operating point is typically set to the half-gain point of the BGS.

By changing the pump modulation format, the shape of the BGS can be manipulated to make it more suitable for dynamic, slope-assisted measurements [13]. Specifically, using a phase-modulated (PM) pump [8], the BGS shape is determined by the phase shift induced by the Brillouin interaction [10]:

$$g_p(\nu) = g_{B0}\frac{2\Delta_\nu \Delta\nu_B^2}{\Delta\nu_B^2 + 4\Delta\nu^2} \tag{2}$$

As indicated in Fig. 1 (red curve), the setpoint with a PM pump can be set to the zero-gain point. The resulting sensitivity (i.e., the BGS slope) is approximately twice the sensitivity achieved with an IM pump. However, this result is only valid if comparing pump waves having the same modulation depth. In actual conditions, this may be not true because of the different characteristics of the devices used to modulate the pump.

III. Experimental Results

Experiments were performed using the BOFDA scheme shown in Fig. 2 [14]. The output from an external-cavity diode laser (ECDL) is first split in two branches for pump and probe generation. The light in the probe branch is passed through an electro-optic modulator (EOM2) biased at its null-point and driven by a microwave generator, generating two first-order sidebands. The two sidebands are first amplified by an Erbium-doped fiber amplifier (EDFA), then are passed through a narrowband fiber Bragg grating (FBG) filtering out one of the two sidebands, as well as the Amplified Spontaneous emission (ASE) noise introduced by the EDFA. The remaining sideband is then injected into the FUT. In the other arm, the pump light is modulated through either an intensity, or a phase modulator (EOM1). In both cases, the modulator is driven by the output port of a vector network analyzer (VNA), boosted up to +26 dBm through an RF amplifier. The modulated pump is then amplified by another EDFA, before being injected to the other end of the FUT. A polarization switch (PS) is also employed to compensate the Brillouin gain fluctuations arising from birefringence [14]. The probe light exiting from the FUT is photo-detected and sent to the VNA for narrowband demodulation. Finally, the demodulated signal is sent to a personal computer for processing. The intermediate frequency (IF) bandwidth of the VNA can be regulated to reduce the noise floor and then increase the SNR, at the expense of a longer sweep time. Other relevant parameters are the frequency step and the maximum frequency used for the VNA frequency sweep, which determine the maximum FUT length and the spatial resolution [8]. In our tests, the modulation frequency was swept up to a maximum of 12 GHz, resulting in a minimum spatial resolution of 8 mm.

While BOFDA sensors provide excellent spatial resolution capabilities, the measurement accuracy may be negatively affected by pump depletion [17], which distorts the BGS in the last part of the FUT. This effect is negligible in our experiments, where a polyamide-coated, single-mode FUT with a total length of only ≈16 m was used. For much longer fibers (several km's), some compensation method based, e.g., on the use of a dual-sideband probe may be used to reduce the influence of nonlocal effects [17].

A small piece of the FUT was fixed through silicone thermal grease to a 10-mm Peltier cell connected to a PID controller. A 3-mm thermistor was also fixed along the border of the Peltier cell, using the same thermal grease. Using the thermoelectric system formed by the Peltier cell, the thermistor and the PID controller, the temperature of the fiber fixed to the Peltier cell could be controlled with a precision better than 0.1 °C. A proper temperature profile was programmed on the PID, in order to vary the temperature from 29°C to 32°C at 1°C temperature steps, while recording the Brillouin gain variations (50 acquisitions per temperature value) using the setup in Fig. 2.

At first, a static measurement of the BGS along the FUT was performed after setting a measurement range of 50 m, a spatial resolution of 8 mm and IF bandwidth of 10 kHz, using both the IM and PM scheme. This measurement was necessary to determine the optimal setpoint for the subsequent, dynamic tests [10], [11], [12]. In Fig. 3 we show the BGS acquired at the hotspot position, using the two configurations, with the Peltier cell set at 29 °C. As marked in the figure, the BGS

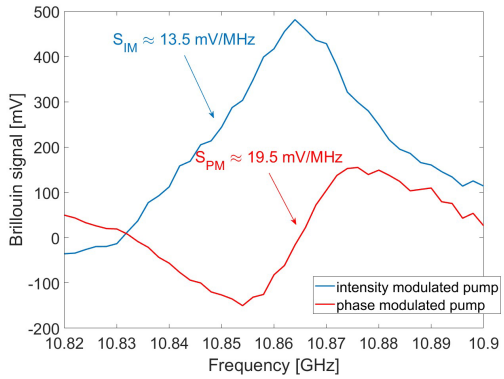

Fig. 3. Brillouin gain spectrum (BGS) acquired for an IM (blue curve) or PM pump (red curve).

slope around the setpoint chosen for the dynamic tests was ≈ 13.5 mV/MHz for the IM BGS, and ≈ 19.5 mV/MHz for the PM BGS. The sensitivity ratio is then ≈ 1.44, quite below the numerically determined 2-factor. As already pointed out, such discrepancy can be explained considering the different efficiency of the two modulators used to modulate the pump.

Based on the results shown in Fig. 3, the pump-probe frequency shift was set to 10850 MHz for the IM pump measurements, and 10865 MHz for the PM pump measurements. Dynamic tests were performed by recording the baseband TF of the FUT at the selected probe frequency and performing an IFFT to transform the measurement data into the spatial domain. Finally, the time evolution of the Brillouin gain at the hotspot position was acquired over consecutive acquisitions. We show in Figs. 4(a) and (b) the temperature acquired at the hotspot position, as well as at a 16-mm distant position, using the two analyzed BOFDA configurations and the thermistor. In both cases, the Brillouin gain was converted to temperature by applying the calibration factor determined through the static measurement and adding a proper offset. A BFS sensitivity to temperature of 1 MHz/°C was assumed. The reported data have been acquired using the same parameters set for the static measurement shown in Fig. 3, resulting in a slope-assisted acquisition rate of 0.49 Hz. For completeness, we also show in Fig. 4(c) the calibration curve for the IM and PM configurations. From Figs. 4, we first note that fiber measurements exhibit some over- and undershoots, which are not visible in the thermistor measurements. The discrepancy is probably due to the longer gauge length and lower thermal capacity of the fiber sensor, compared to the thermistor. Second, the PM measurements are apparently less noisy than IM measurements. We can assess the different performance by computing the standard deviation (STD) of the temperature measurements over the regions at constant temperature. The resulting STDs are 0.25 °C for the IM data, and 0.15 °C for the PM data. Assuming that the SNR is inversely proportional to the measurement STD [15], the SNR difference between the two methods, for this test, was 2.3 dB. Note that, this value is even larger than the slope ratio previously determined from the static measurements (1.44, i.e., ≈ 1.60 dB). Further analyses are necessary to determine the causes of this extra SNR enhancement.

Another observation is that the FUT temperature values show a small systematic error (see e.g., the data at T = 32°C

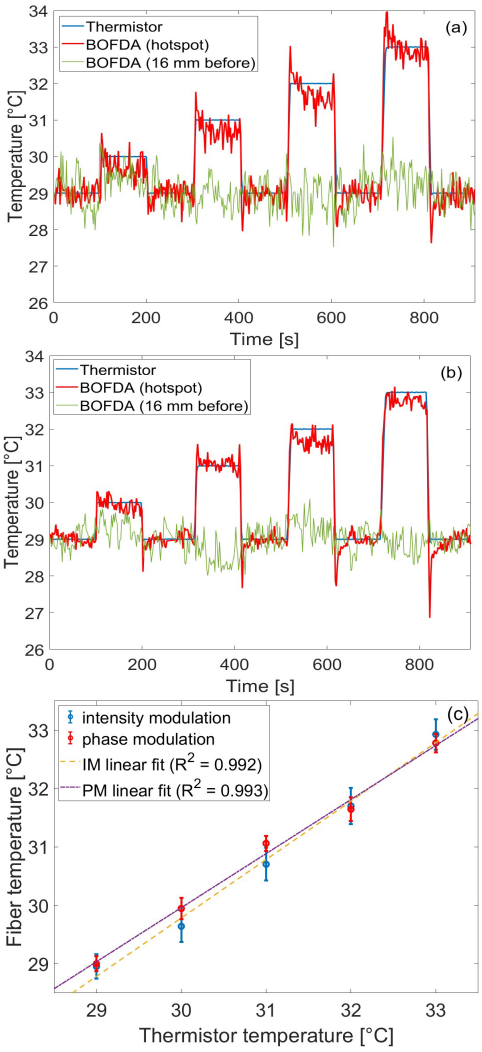

Fig. 4. Temperature measurements with IM (a) or PM pump (b), and temperature calibration curves (c).

in Fig. 4b). This may be attributed to some nonlinearity in the fiber response (see Fig. 3), which may be corrected by using a nonlinear (e.g., quadratic) calibration curve. Finally, we observe that the reported performances are significantly better than those reported in [7], even for the IM scheme. This is explained by considering that, at the liquid nitrogen temperature, the reduced sensitivity of the BFS to temperature and the larger BGS bandwidth led to a penalty factor of ≈15 in slope-assisted measurements [7]. We also underline that, the results presented here have been obtained without applying any filter to the measurements, while for [7] a wavelet-denoising filtering was applied to the raw data.

In order to analyze the influence of the measurement parameters on the sensor performance, the same temperature cycle was applied while performing the measurement at varying measurement range (50 m or 25 m), spatial resolution (8 mm or 16 mm) and IF bandwidth (10 kHz, 100 kHz or 1.2 MHz). It is noted that, for the measurements carried out with a spatial resolution of 16 mm the fiber was disposed diagonally across the Peltier cell, to heat a ≈14-mm-long piece of fiber. The results are summarized in Table I. For each parameter set, we report the STD of the temperature data acquired using

TABLE I
ANALYSIS OF PERFORMANCE FOR DIFFERENT MEASUREMENT PARAMETERS

Spatial resolution [mm]	Measurement range [m]	IF bandwidth [kHz]	STD (IM) [°C]	STD (PM) [°C]	ΔSNR [dB]	Slope ratio [dB]	Acquisition rate [Hz]
8	50	10	0.25	0.15	2.30	1.60	0.49
8	50	100	0.41	0.20	3.17	1.43	1.56
8	50	1200	1.80	0.74	3.86	2.86	2.30
8	25	10	0.31	0.14	3.39	4.03	0.90
8	25	100	0.65	0.30	3.41	2.22	2.40
8	25	1200	1.42	0.57	3.95	2.79	3.24
16	50	10	0.21	0.12	2.35	1.22	0.97
16	50	100	0.47	0.18	4.22	1.56	2.61
16	50	1200	1.47	1.01	1.65	1.22	3.34
16	25	10	0.24	0.14	2.33	1.46	1.66
16	25	100	0.68	0.35	2.96	1.03	3.61
16	25	1200	2.14	0.59	5.58	5.95	4.36

either the IM or PM scheme. The same table also reports the SNR improvement resulting from the use of the PM pump; the ratio between the BGS slope at the operating point as determined experimentally for the two modulation schemes and the acquisition rate. Comparing the SNR enhancements and the slope ratios, we note that, as in the measurement discussed before, the former is typically larger than the latter, confirming that the PM scheme provides an extra SNR enhancement that cannot be explained only in terms of the larger slope of the BGS at the selected setpoint. The SNR improvement ranges from 1.65 dB to 5.58 dB, depending on the experimental conditions, with an average value of 3.3 dB. From the table we also note that, as expected, the temperature accuracy is improved by setting a coarser spatial resolution and a smaller IF bandwidth, while the effect of the measurement range is less evident. In any case, the measurements carried out with an IF bandwidth of 1.2 MHz tended to be very noisy, and therefore even the estimated temperature STD is less reliable due to the higher uncertainty in the estimation of the BGS slope.

Note that, while in the present case the fiber was only subject to temperature variations, in field applications the strain may affect the BFS as well, leading to potential false alarms in hotspot detection. This may be avoided by using a FUT with multiple Brillouin gain peaks, each one with a different sensitivity to temperature and strain [18]: Acquiring the Brillouin gain at the slope of each peak, would allow strain compensation at the expense of the acquisition time. Alternatively, one may also combine the present technique with a Rayleigh scattering method for strain/temperature discrimination [19].

IV. CONCLUSION

A slope-assisted BOFDA scheme was used to perform high-resolution hotspot measurements in a single-mode optical fiber at room temperature. Using a phase-modulated pump we have demonstrated an average ≈3-dB improvement of the SNR, compared to a conventional scheme based on an IM pump. While the reported performances are still inferior to those offered by commercial instruments based on Rayleigh scattering, especially in terms of acquisition rate (see e.g., [16]), the proposed sensor has some advantages such as absolute temperature measurement capabilities, a potentially longer measurement range, and reduced susceptibility to vibration-induced noise. The proposed sensor can be usefully applied for quench detection in superconducting magnet systems, although further tests are necessary to assess its effectiveness at cryogenic temperatures. Furthermore, our technique can be generally applied in other hotspot detection applications, such as in photovoltaic cells, power cables and electrical generators.

REFERENCES

[1] A. H. Hartog, *An Introduction to Distributed Optical Fibre Sensors*. Boca Raton, FL, USA: CRC Press, 2018.
[2] E. E. Salazar et al., "Fiber optic quench detection for large-scale HTS magnets demonstrated on VIPER cable during high-fidelity testing at the Sultan facility," *Superconductor Sci. Technol.*, vol. 34, no. 3, Mar. 2021, Art. no. 035027.
[3] F. Scurti, S. Ishmael, G. Flanagan, and J. Schwartz, "Quench detection for high temperature superconductor magnets: A novel technique based on Rayleigh-backscattering interrogated optical fibers," *Superconductor Sci. Technol.*, vol. 29, no. 3, Jan. 2016, Art. no. 03LT01.
[4] S. Mahar et al., "Real-time simultaneous temperature and strain measurements at cryogenic temperatures in an optical fiber," *Proc. SPIE*, vol. 7087, Aug. 2008, Art. no. 70870I.
[5] R. Bernini, L. Crocco, A. Minardo, F. Soldovieri, and L. Zeni, "All frequency domain distributed fiber-optic Brillouin sensing," *IEEE Sensors J.*, vol. 3, no. 1, pp. 36–43, Feb. 2003.
[6] K. Hotate and M. Tanaka, "Distributed fiber Brillouin strain sensing with 1-cm spatial resolution by correlation-based continuous-wave technique," *IEEE Photon. Technol. Lett.*, vol. 14, no. 2, pp. 179–181, Feb. 2002.
[7] A. Minardo, E. Catalano, R. Vallifuoco, L. Zeni, and R. Bernini, "Distributed cryogenic temperature sensing through Brillouin optical frequency-domain analysis," *Proc. SPIE*, vol. 12643, May 2023, Art. no. 126432D.
[8] A. Minardo, G. Testa, L. Zeni, and R. Bernini, "Theoretical and experimental analysis of Brillouin scattering in single-mode optical fiber excited by an intensity- and phase-modulated pump," *J. Lightw. Technol.*, vol. 28, no. 2, pp. 193–200, 2010.
[9] D. Garus, T. Gogolla, K. Krebber, and F. Schliep, "Distributed sensing technique based on Brillouin optical-fiber frequency-domain analysis," *Opt. Lett.*, vol. 21, no. 17, pp. 1402–1404, 1996.
[10] J. Urricelqui, A. Zornoza, M. Sagues, and A. Loayssa, "Dynamic BOTDA measurements based on Brillouin phase-shift and RF demodulation," *Opt. Exp.*, vol. 20, no. 24, pp. 26942–26949, 2012.
[11] R. Bernini, A. Minardo, and L. Zeni, "Dynamic strain measurement in optical fibers by stimulated Brillouin scattering," *Opt. Lett.*, vol. 34, no. 17, pp. 2613–2615, 2009.
[12] Y. Peled, A. Motil, L. Yaron, and M. Tur, "Slope-assisted fast distributed sensing in optical fibers with arbitrary Brillouin profile," *Opt. Exp.*, vol. 19, no. 21, pp. 19845–19854, 2011.
[13] G. Yang, X. Fan, B. Wang, and Z. He, "Enhancing strain dynamic range of slope-assisted BOTDA by manipulating Brillouin gain spectrum shape," *Opt. Exp.*, vol. 26, no. 25, pp. 32599–32607, 2018.
[14] R. Bernini, A. Minardo, and L. Zeni, "Distributed sensing at centimeter-scale spatial resolution by BOFDA: Measurements and signal processing," *IEEE Photon. J.*, vol. 4, no. 1, pp. 48–56, Feb. 2012.
[15] M. A. Soto and L. Thévenaz, "Modeling and evaluating the performance of Brillouin distributed optical fiber sensors," *Opt. Exp.*, vol. 21, no. 25, pp. 31347–31366, 2013.
[16] *ODiSI 6000 Data Sheet*. Accessed: Dec. 12, 2023. [Online]. Available: https://lunainc.com/sites/default/files/assets/files/data-sheet/Luna%20ODiSI%206000%20Data%20Sheet.pdf
[17] A. Minardo, R. Bernini, and L. Zeni, "A simple technique for reducing pump depletion in long-range distributed Brillouin fiber sensors," *IEEE Sensors J.*, vol. 9, no. 6, pp. 633–634, Jun. 2009.
[18] X. Liu and X. Bao, "Brillouin spectrum in LEAF and simultaneous temperature and strain measurement," *J. Lightw. Technol.*, vol. 30, no. 8, pp. 1053–1059, Apr. 2012.
[19] D.-P. Zhou, W. Li, L. Chen, and X. Bao, "Distributed temperature and strain discrimination with stimulated Brillouin scattering and Rayleigh backscatter in an optical fiber," *Sensors*, vol. 13, no. 2, pp. 1836–1845, Jan. 2013.

Open Access funding provided by 'Università degli Studi della Campania "Luigi Vanvitelli"' within the CRUI CARE Agreement